Nanoscale

Accepted Manuscript

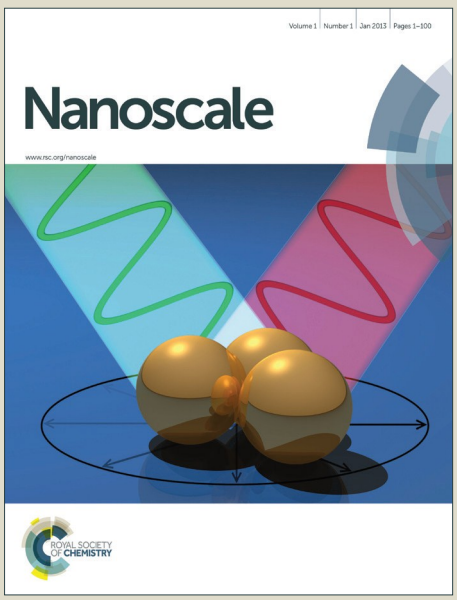

ROYAL SOCIETY OF CHEMISTRY

www.rsc.org/nanoscale

Journal Name

RSCPublishing

ARTICLE

High pressure pyrolyzed non-precious oxygen reduction catalysts for alkaline polymer electrolyte membrane fuel cells

Jakkid Sanetuntikul and Sangaraju Shanmugam*,

Cite this: DOI: 10.1039/x0xx00000x

Received 00th January 2012,
Accepted 00th January 2012

DOI: 10.1039/x0xx00000x

www.rsc.org/

Non-precious catalysts such as metal-coordinated with nitrogen doped-carbons have showed reasonable oxygen reduction reaction (ORR) in alkaline fuel cell. In this report, we present the development of highly active and stable low-cost non-precious ORR catalyst by direct synthesis under autogenic-pressure conditions. Transmission electron microscope studies show highly porous Fe-N-C and Co-N-C structures, which further confirmed by Brunauer-Emmett-Teller surface area measurements. The surface area of Fe-N-C and Co-N-C catalysts were found to be 377.5 and 369.3 m^2 g^{-1}, respectively. XPS results show possible existence of N-C and M-N_x structure, which are generally proposed to be the active sites in non-precious catalyst. Fe-N-C electrocatlyst exhibits the ORR half-wave potential, 20 mV higher than reference Pt/C catalyst. The cycling durability test for 5,000 cycles of Fe-N-C shows the half-wave potential loss only 4 mV, whereas Pt/C catalyst showed about 50 mV. The Fe-N-C exhibited improved activity and stability compared to the reference Pt/C and possess direct 4-electron transfer pathway for ORR process. Further, the Fe-N-C catalyst provides extremely low HO_2^- production as confirmed by rotating ring-disk electrode measurement. In alkaline fuel cell single cell test, a maximum power density of 75 and 80 mWcm^{-2} was observed for Fe-N-C and Pt/C cathodes, respectively. Durability studies (100-h) show decay of fuel cell current was more prominent for Pt/C than Fe-N-C cathode based catalyst. Therefore, the Fe-N-C catalyst appears to be a promising new class of non-precious catalyst prepared by an autogenic synthetic method.

Introduction

Electrochemical oxygen reduction is the key reaction for the energy conversion technologies.[1–4] Currently, polymer electrolyte fuel cells have paid great attention to use non-precious catalyst for oxygen reduction reaction (ORR) to replace the Pt-based catalysts and reduce the cost of fuel cell technology. Therefore, significant research has been focused on the development of non-precious catalyst, owing to their high activity, stability, and possible to use in wide range of pH.[5–7]

The research on non-precious catalyst has been continually pursued since the key research initiated by Jakinski,[8] who used metal phthalocyanines based catalysts for the ORR in an alkaline medium. In later studies, the development of highly active and durable non-precious catalyst based on heteroatom doped-carbon[9–12] or metal coordinated with nitrogen-doped carbon (M-N-C, M = Fe, Co or FeCo) synthesized by heat-treatment of various precursors from 700 to 1,000˚C under an inert gas atmosphere, resulting the ORR catalyst with superior activity and stability.[9–11,13] Some of excellent examples non-precious catalysts are described by Chung *et al.*[14] using iron acetate as a metal source/cyanamide as nitrogen source/functionalize black pearls (carbon 2000) as a carbon source, then direct pyrolysis at high temperature under N_2 atmospheres. This catalyst exhibits good stability and activity better than Pt/C with high loading at 1 mg cm^{-2} with and presence of Fe-N_4 active sites are responsible for the significant improvement of ORR activity. Wu *et al.*[15] reported a highly active ORR catalyst, which showed comparable activity to that of commercial Pt/C and exhibited a superior durability up to 700h at 0.4V. This catalyst was synthesized using Fe(III) chloride/polyaniline (PANI)/Ketjenblack, then the solid mixture was heat-treated under N_2 atmosphere at 900 ˚C, then acid-treated in 0.5 M H_2SO_4 at 80°C for 8 hours to remove any unstable phases, then the precipitate catalyst underwent a second heat treatment under N_2 as the final step of the synthesis. Tan *et al.*[16] fabricated MnO-mesoporous-N-C composite by first mixing precursor $Mn(NO_3)_2$/aniline/$KMnO_4$ in autoclave, then the solid precipitate was collected and then pyrolysed under Ar atmosphere at 900˚C for 4h. The resultant product was treated with acid, washed and dried before further characterization. They found that the half-wave potential of MnO-mesoporous-

N-C catalyst showed 50 mV lower than Pt/C catalyst. Proietti *et al*.[17] was created an excellent M-N-C catalyst by mixture of ferrous acetate/phenanthroline/ metal-organic framework (MOF) followed by direct pyrolysis, first under Ar then under ammonia atmosphere to obtain the electroctalyst. The highly porous cathode catalyst showed power density of 0.75W cm^{-2} at 0.6 in H_2-O_2 single cell system, which is comparable with a commercial Pt-based catalyst and excellent stability even in H_2-Air system. According to the aforementioned issues, it is well known that to obtain non-precious catalyst based carbon via pyrolysis of precursors via contain metal-nitrogen-carbon have been demonstrated to provide active ORR catalyst. However, the pyrolysis of precursor is usually synthesized at high temperature under inert gas atmosphere, which prevented the complete decomposition of carbon mass, leading to a poor catalyst ORR based carbon.

We initiated a research effort to develop excellent M-N-C electrocatalyst with synergetic of porosity that improved an active-site density, O_2 transport and ion-conduction under highly autogenic-pressure method at high temperature without using any inert gas atmosphere. The ORR activity of Fe-N-C, was quantified from rotating disk electrode (RDE) and rotating ring disk electrode (RRDE) measurements, and the obtained results were correlated with active sites of N-C, and M-N_X to provide electrode material characteristics, which are responsible for high ORR activity. Further, we constructed a membrane electrode assembly using M-N-C as cathode catalyst using alkaline membrane and results are presented. In this report, we propose the synthesis of Fe-N-C and Co-N-C catalyst by autogenic-pressure method. Neither N_2, NH_3 nor Ar atmosphere was used during pyrolysis in first heat-treated or second heat-treated. The Fe-N-C and Co-N-C prepared by this method show superior activity and stability under alkaline environment.

Experimental

Preparation of electrocatalysts

The M-N-C electrocatalysts were prepared by facile direct pyrolysis under autogenic pressure condition. First, we have synthesized a precursor by mixing of melamine (3.5 g), iron acetate or cobalt acetate (1.0 g), and oxidized carbon powder (1.0 g) (VXC-72R in 60% nitric acid at 90˚C for 6h) were stirred together in ethanol at 60˚C overnight. Then the solvent was evaporated at 45˚C and remaining powder was converted to electrocatalyst using direct pyrolysis under autogenic-pressure with Swagelok union closed cell at 900˚C for 1 h with heating rate 10˚C min^{-1}. One hundred milligrams of as-synthesized precursor was acid treated in 5mL of 0.5M H_2SO_4 at 90˚C for 6h to remove unreacted metallic compounds and then washed with copious amount of water till pH becomes neutral, then the product was dried overnight in vacuum oven. In the final step, the acid treated catalyst was heat-treated for the second time using Swagelok closed cell at 900˚C for 1 h, resulted in Fe-N-C and Co-N-C catalyst.

Physical characterization of catalysts

The morphology of the catalysts was analyzed by the field-emission scanning electron microscope (FE-SEM, Hitachi, S-4800II) with an accelerating voltage of 3 kV. Before the SEM observation, the samples were coated with Osmium in vacuum chamber. The microstructures of samples were determined by field-emission transmission electron microscope (FE-TEM, Hitachi, HF-3300) with an acceleration voltage of 300 kV. For TEM analysis, samples were ultrasonically dispersed in isopropyl alcohol, and then a drop of dispersion was deposited on copper grid and dry under UV lamp. The crystal structure of samples was investigated by powder X-ray diffraction (XRD, Panalytical-Empyrean) using Cu Kα radiation at a generator voltage of 40 kV and a tube current of 30 mA. Raman spectra were obtained by using Thermo Nicolet ALMECA XR, Thermo Scientific at 514 nm excitation lasers and the sample powder were prepared on glass surface with laser focused through 100X microscope for total interrogation spot size of 1 micron. Crystal structure and elemental analysis studies performed by X-ray photoelectron spectroscope (XPS, Thermo Fisher Scientific, ESCALAB250 XPS system, Theta Probe XPS system) using monochromated Al K-alpha source at 15 kV and 150 W. Binding energy values at X-axis were calibrated using C1s from a carbon value taken as 284.6 eV.

Electrochemical characterization of catalysts

The ORR activity of electrocatalyst was carried out using rotating disk electrode (RDE) and rotating ring-disk electrode (RRDE) techniques using Biologic, VSP. A three electrode system consisting of the glassy carbon, Pt wire and standard calomel electrode (SCE) act as working electrode, counter and reference electrodes, respectively. All potential were converted to RHE scale by adding 0.991V, according to literature experiment.[18,19] The catalyst ink for the electrochemical measurements was prepared by dispersing 5 mg of the catalyst in 250 µL DI-water, 20 µL of Nafion (5%), and 500 µL isopropyl alcohol, then ultrasonication for 30 min to obtained homogenous ink. From this, the catalyst ink was loaded on a clean glassy carbon electrode with 0.6 mg cm^{-2} and 0.4 mg cm^{-2} for RDE and RRDE experiment, respectively. The catalyst loading for reference Pt/C electrode was 30 µg cm^{-2} in both cases. The ORR experiment was carried out in O_2-saturated 0.1M KOH electrolyte at a scan rate 10mV s^{-1} at ambient temperature. A flow of O_2 was maintained over the electrolyte during the measurement to ensure O_2 atmosphere inside the cell. For comparison, the commercial reference Pt/C (10 wt%, Johnson-Matthey) was used for the half-cell studies.

Fuel Cell Testing

The alkaline fuel cell evaluated by making membrane electrode assemblies (MEAs). The commercial alkaline exchange membrane (Tokuyama, A201) was used to make MEA. The membrane was treated by dipping in 1M KOH for 24h, then washed with DI-water until pH was neutral. The catalyst ink was prepared by dispersing catalyst powder with DI-water, and 40

wt% ionomer solution (Tokuyama, AS-4 ionomer) followed by isopropyl alcohol. The resultant homogeneous ink was accomplished by ultrasonicating the contents for 30 min. The catalyst layer, 40 wt % Pt/C catalyst (Johnson Matthey) and Fe-N-C catalyst were used as anode and cathode, respectively. The catalyst was brushed onto diffusion-layer coated carbon papers (SGL, thickness = 0.27mm) to make diffusion-electrode. The anode catalyst loading was 0.5 mg_{pt} cm^{-2}. The cathode catalyst, Fe-N-C loading was 4 mg cm^{-2}. For comparison, a reference cathode catalyst, 40 wt% Pt/C was prepared in a similar manner to anode. Single cell MEA was obtained by comprising the membrane between the cathode and anode followed by hot-compressing at 80°Cand 15 kg cm^{-2} for 2 min. Fuel cell performance was carried out at 60˚C by passing humidified H_2-O_2 (100% RH, flow rate, 0.4L min^{-1}). Before conducting the polarization plots, the MEAs were left at open-circuit voltages condition for 3 h under 100 %RH, till the system reach to steady state point. All the MEAs were evaluated in single cells under atmospheric pressure without applying any back pressure.

Result and discussion

Fig. 1a and b shows the SEM images of Fe-N-C and Co-N-C catalysts reveal high porosity, uniform particle size distribution and no agglomeration. The diameter of particles is about 30 nm, which corresponds to the size of VXC-72R carbon structure, as further evidenced by TEM images (Fig. 1c and d). Furthermore, the TEM images reveal some small metal particles encapsulated in porous carbon.

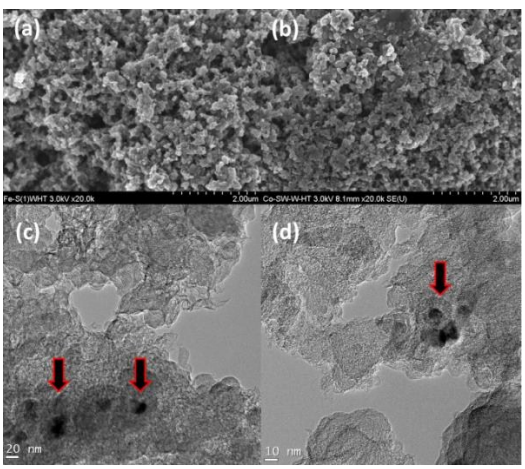

Figure 1. Typical micrographs of (a) Fe-N-C and, (b) Co-N-C catalysts. HRTEM images of (c) Fe-N-C and (d) Co-N-C catalysts, where the arrows in each image designate the catalyst containing metal nanoparticles.

The X-ray diffraction (XRD) was carried out for the acid treated Fe-N-C and Co-N-C catalysts to determine the crystalline structure (Fig. 2a). XRD patterns of two catalysts show a broad graphitic C(002) and C(100) peaks, indicates a typical turbostratic carbon structure.[20] The C(002) plane of Fe-N-C and Co-N-C was found to be at 24.5˚ and 24.9˚ respectively. The shift to lower angle (2Θ) of C(002) plane suggests an increase in the interlayer-distance that related to the N-doping in carbon structure, and may further doping of Fe atom as well.[21] To evaluate the nature of carbon structure, Raman spectra was acquired for Fe-N-C and Co-N-C catalysts. The Raman spectra show the characteristic carbon peaks at ~1360 cm^{-1} (D-band) and ~1590 cm^{-1} (G-band) as shown in Fig. 2b. The D-band corresponds to sp^3 defect site while G-band relate to the sp^2-hybridized on carbon layer.[22] The ratio of I_D and I_G bands (I_D/I_G) was used to identify the overall quality of carbon present in the catalyst. The value of I_D/I_G ratios for Fe-N-C and Co-N-C were 0.91 and 0.89, respectively. Surface area properties are very important for the electrochemical catalyst for ORR. The Brunauer-Emmett-Teller (BET) surface area of the Fe-N-C and Co-N-C samples were found to be 377.5 and 369.3 m^2 g^{-1}, respectively. According to IUPAC guideline, an average pore size between 2 and 50 nm is termed as mesoporous materials. The pore size distribution of Fe-N-C and Co-N-C catalysts showed the pore size of 3.61 and 3.63 nm, respectively. This result indicates the presence of mesoporous in M-N-C catalysts.

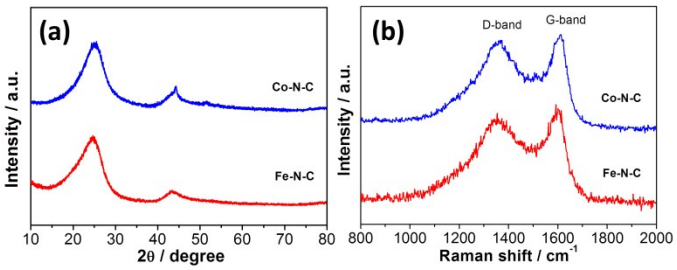

Figure 2. (a) XRD patterns, and (b) Raman spectra of Fe-N-C and Co-N-C catalysts.

The XPS survey spectra of Fe-N-C and Co-N-C catalysts revealed the presence of Fe, Co, C, O, and N (Fig S5, ESI†). The spectra in Fig. 3a shows a broad $Fe2p_{3/2}$ peak, it can deconvoluted into two peaks with a binding energy values of 712.8 and 710.1 eV, which can be assigned to Fe(II) ion[21] and Fe(III) ion[23], respectively. Fig.3b shows the $Co2p_{3/2}$ broad peak, which is fitted into two peaks with binding energy values of 780.3 and 782.3 eV, assigned to Co(II)O[24] and Co-N_x[24,25] respectively. The XPS data confirmed that no zero valent metals are observed, it may exists as Fe(II), which bond to the N forming M-N_x species. The corresponding fitting results are given in Table. S1, ESI†. The total nitrogen content measured by XPS of Fe-N-C and Co-N-C catalysts are found to be 3.08 and 1.31 at %, respectively. High resolution N1s spectra was deconvoluted into three peaks with a binding energy values of 398.3, 400.9, and 403.2 eV for Fe-N-C and Co-N-C, which can be assigned to the pyridinic-type,[19,26] pyrolic-type[27] and graphitic-type[28] of nitrogen functional groups, respectively. In fact, the peak at 398.3 eV may also include the presence of N-bond with metal, the pyridinic N (398.0-398.5 eV) bond with N-metal (398.6-398.9 eV) is very difficult to distinguished, so Fe-N-C catalyst showed higher pyridinic-type nitrogen (35.7%) content than Co-N-C catalyst (24.4%). As discussed above, this correlates well with the ORR results, which will be discussed in later section. Furthermore, the quantitative analyses of M-N-C

samples reveal the ratio of N to C (N/C ratio) of Fe-N-C and Co-N-C was found to be 0.033% and 0.014%, respectively. The N/C ratio observed in XPS is in good agreement with the results observed by the element analysis (Table S1 & S2, ESI†).

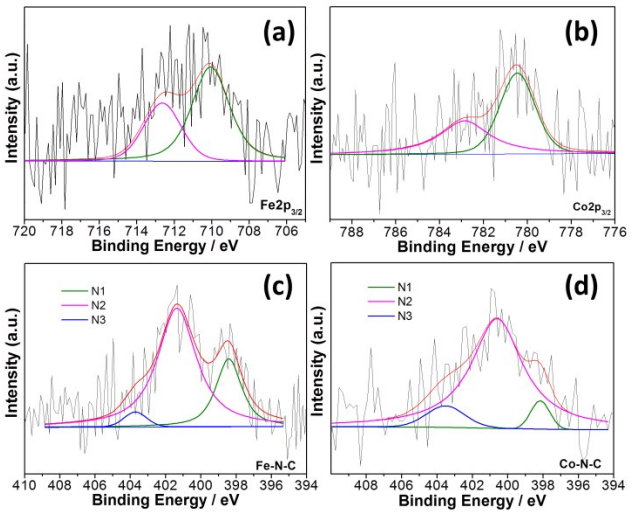

Figure 3. High resolution XPS for (a) $Fe2p_{3/2}$ (b) $Co2p_{3/2}$ and N1s spectra of (c) Fe-N-C , and (d) Co-N-C catalyst.

To evaluate the ORR performance of Fe-N-C and Co-N-C catalysts, the rotating-disk electrode (RDE) was performed in O_2-saturated 0.1M KOH solution at a scan rate 10 mV s^{-1} (Fig4.a and b). The ORR polarization curves recorded from 800 to 2,500 rpm, show the increased current by increasing the rotating speed explained by shortening flux-diffusion resulting increasing the currents. The results were compared with a commercial Pt/C catalyst (10%Pt/C, Johnson Matthew). Fig. 4c shows the comparison of the ORR properties of non-precious catalysts with that of Pt/C catalyst in 0.1M KOH at 1,600 rpm. The ORR onset potential of Fe-N-C catalyst is nearly same as reference Pt/C catalyst with loading 30 μg_{Pt} cm^{-2} (1.05V vs. RHE) and higher than Co-N-C. More importantly, the half-wave potentials ($E_{1/2}$) of Fe-N-C and Co-N-C catalysts are 0.86 and 0.81 V vs. RHE, respectively, while the Pt/C shows an $E_{1/2}$ value at 0.84V. The $E_{1/2}$ of Fe-N-C catalyst is 20 mV higher than Pt/C catalyst and 50 mV higher than Co-N-C catalyst. The addition of transition metal element leads to activity enhancement of the catalysts relative to the nitrogen-doped functionalized VXC-72R carbon (N-C) catalyst as shown in Fig 4c. The Koutecky-Levich (K-L) plots shown in inset Fig. 4a and b are derived from polarization curves and these plots showed a good linearity and parallelism over all the potential range, suggesting first order reaction kinetic of oxygen reduction. The electrons transfer number (n) of are 3.96 and 3.91 for Fe-N-C and Co-N-C catalyst at 0.5V vs. RHE, respectively, suggesting that both catalyst exhibited a direct four-electron process.[29] From these results, the enhanced ORR activity of Fe-N-C catalyst is attributed to i) the total doped-nitrogen content in the carbon network (N/C ratio) of Fe-N-C is higher than Co-N-C, ii) Fe-N-C catalyst exhibits a higher pyridinic-type nitrogen content, which is considered to be an ORR active sites and, iii) Based on XPS data, the Fe and Co contents in the M-N-C catalyst are quite similar. However, Fe-N-C catalyst exhibited higher N-content. So, the probability of creating the M-N_x moieties or N-C in Fe-N-C catalyst is higher than Co-N-C.

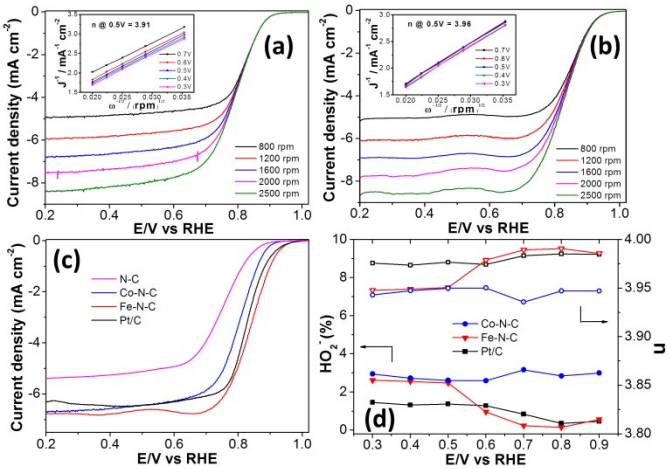

Figure 4. Polarization curves of (a) Co-N-C and (b) Fe-N-C catalysts in O_2-saturated at different rotation speed. (c) LSVs curve for Co-N-C, Fe-N-C, and Pt/C in O_2-saturated at 1,600 rpm, 0.1M KOH, and (d) electron transfer number and percentage of peroxide formations of catalyst at different potential obtained from RRDE experiment. Inset in (a) and (b) are Koutecky-Levich plots of Co-N-C and Fe-N-C, respectively.

Adding metal precursor during the synthesis showed the enhancement for the ORR performance better than N-doped carbon. The introduction of M atom is more likely to create M-N_4 moiety developed in the catalyst. Generally, the metal-ion centers considered to be more active ORR, which could be correlated to the increased binding capabilities form oxygen and higher ionization potentials. We can conclude that Fe-N-C is highly active catalyst, indicating the synthesis of electrocatalyst under autogenic pressure is appears to be a promising method to synthesize the Fe-N-C catalyst and activity of such catalyst is comparable with other ORR catalysts based on carbon nanotube (CNT),[14] porous[29] or graphene[30] as well. In fact, we have also tested the ORR activity of Fe-N-C catalyst under acidic electrolyte condition, which showed good diffusion-limited current and $E_{1/2}$ potential is only 50mV lower than the reference Pt/C catalyst (Fig. S6, ESI†).

The formation of peroxide species (HO_2^-) during the ORR process was analyzed by rotating-ring disk electrode (RRDE). The ring and disk current recorded at 1,600 rpm in 0.1M KOH with O_2-saturated for Fe-N-C and Co-N-C catalyst was compared with reference Pt/C (Fig. S7, ESI†). The percentage of HO_2^- and the number of electron transferred (n) derived from RRDE experiments are the same value of ~3% and ~3.95, respectively over the potential 0.3-0.9 V, which is in good agreement with the electron transfer number observed from RDE experiments. Interestingly, Fe-N-C and Co-N-C catalysts exhibit extremely low HO_2^- and higher number electron transfer in alkaline condition.

For the ORR process of non-precious catalyst, oxygen molecule can reduce to HO_2^- at M-N-C or N-C active site and further reduce again at metal-oxide site as suggested by Mukerjee *et al*.[31], a bi-functional mechanism can be observed. The ORR process mainly occurs at Fe-N_x and Co-N_x, then the intermediate HO_2^- can be also captured as well by metal-oxide particle which encapsulated directly in the carbon porous (see TEM images in Fig. 1 and Fig. S2, ESI*). A similar report has been published by Liang *et al*.[32], where the interaction of N-graphene and Co_3O_4 on Co_3O_4/N-graphene catalyst composites can improve ORR performance. We believed the highly synergetic of M-N_x and small amount metal-oxide greatly contributes to enhanced ORR performance.

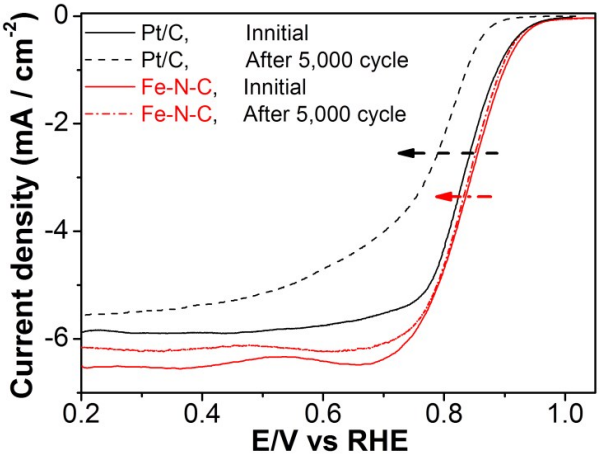

Figure 5. Polarization curves of Fe-N-C and Pt/C during cycling durability test in O_2-saturated at 1,600 rpm (cycling test were carried out in potential range 0.6-1.0V vs RHE with 50mV s^{-1} in 0.1M KOH)

The cycling durability test of Fe-N-C catalyst was carried out and compared with a Pt/C catalyst by performing repeated potentiodynamic cycling for 5,000 cycles with a potential range of 0.6-1.0 V vs. RHE at a scan rate of 50 mV s^{-1} (Fig. 5). After 5,000 cycles, the $E_{1/2}$ of Fe-N-C catalyst showed a small loss about 4 mV while Pt/C catalyst showed 50 mV negative shifts. These results indicated that surface property of non-precious catalyst still maintained during potential cycling test. The degradation of Pt/C and Fe-N-C are different because Pt particle are suffered from Pt agglomeration, Pt dissolution and degradation of carbon support at high potential that lead to degradation of Pt/C catalyst. While Fe-N-C can degrade in case of carbon material and oxidation of active site.[33]

MEA fuel cell test of catalyst is an important for practical application. The comparison of alkaline membrane fuel cells between Fe-N-C (loading: 4mg cm^{-2}) and commercial Pt/C (40% Pt/C-JM, loading: 0.5mg_{Pt} cm^{-2}) as cathode catalyst for single cell H_2-O_2 gases system at 60˚C are shown in Fig.6. The open circuit voltage (OCV) of Fe-N-C, Co-N-C and Pt/C were 1.04, 0.99 and 1.04V, respectively. The maximum power density (P-max) of Fe-N-C, Co-N-C and Pt/C were 75, 68 and 80 mW cm^{-2} for Fe-N-C, Co-N-C and Pt/C catalyst, respectively. The alkaline fuel cell performance of Fe-N-C electrode was almost comparable with Pt/C, further the Fe-N-C catalyst displayed the behaviour like Pt/C in the all current density region, demonstrating the Fe-N-C electrocatalyst afford the highly active in ORR process. This value of P-max compares to other non-precious cathode catalyst result was summarized and listed in Table. S3, ESI†. Although the performance of Fe-N-C and Pt/C as cathode catalyst is low compared with Kruusenberg *et al*.[34] The possibility depending on the cathode catalyst, membrane, modifying fuel cell condition (temperature, humidifying, pressure, flow rate of gas, back pressure, water-transport in electrode) and MEA fabrication techniques have to concern. Further studies are underway using different alkaline exchange membrane and MEA fabrication techniques to measure the power density of M-N-C catalyst.

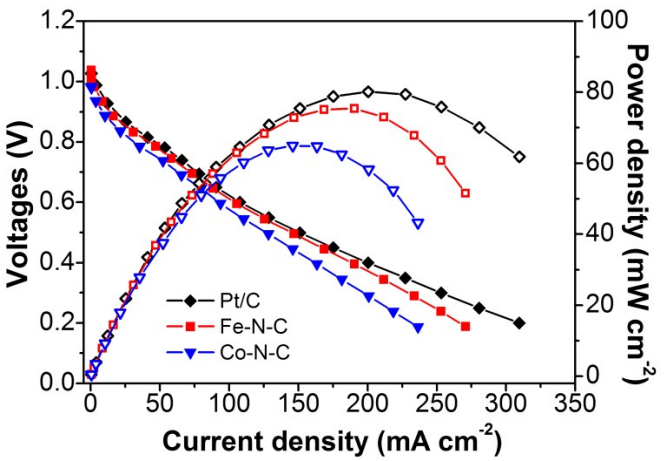

Figure 6. Alkaline membrane fuel cell performance of MEA with Fe-N-C and Pt/C as cathode at 60˚C.

The fuel cell 100-hour durability tests under 100%RH at 60°C, with constant voltage 0.4V for Fe-N-C and reference Pt/C catalysts are shown in Fig. 7. The fuel cell durability test of Pt/C cathode catalyst shows the current decay is faster than Fe-N-C. The best durability was obtained with Fe-N-C, with a drop in current density of only 8% at 0.4 V, while Pt/C shows a loss of ~20%. The high durability of Fe-N-C electrode indicates a promising electrocatalyst for oxygen reduction in alkaline membrane fuel cell. The advance surface characterization studied is needed to clarify for M-N-C active activity and durability of the catalyst is also an important feature must be able to test for more hundreds/thousands of hours within a fuel cell to be considered for applications.

Conclusions

In summary, we present a highly active non-precious ORR catalyst that was prepared by a simple method using direct pyrolysis without purging any gases in a specially made cell. In the synthesis, the nitrogen and metal source, including carbon play an important role to make porous M-N-C electrode materials, resulting strongly induces the ORR active site. The

ORR results reveal that of Fe-N-C catalyst with loading 0.6 mg cm^{-2} showed $E_{1/2}$ potential higher than reference Pt/C

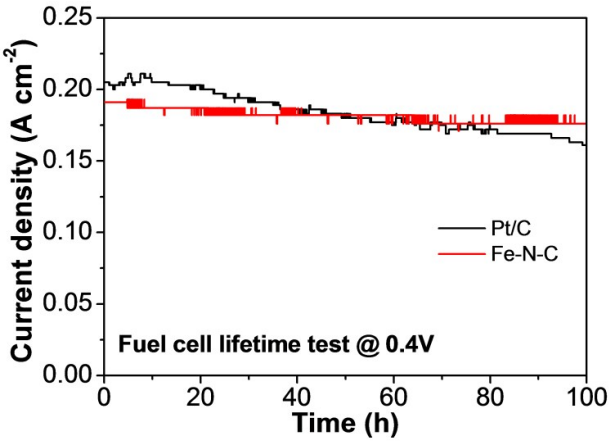

Figure 7. Alkaline membrane fuel cell performance durability test at a constant voltage 0.4V in H_2-O_2 for a MEA with Fe-N-C and Pt/C as cathode based catalyst at 60˚C.

with 30 μg cm^{-2} catalysts loading. Furthermore, the Fe-N-C provides a direct 4-electron pathway and superior durability toward ORR in alkaline medium. In the single cell test, the Fe-N-C as cathode catalyst provides maximum power density is comparable with commercial Pt/C and better long-term stability for 100 h indicates the good activity for the catalyst. The M-N-C catalyst synthesized by this method using inexpensive precursor would be a promising choice as cathode catalyst for fuel cell.

Acknowledgements

The authors would like to acknowledge to DGIST R&D Program of the Ministry of Education, Science and Technology of Korea (15-BD-01) for financially supported.

Notes and references

[a] Department of Energy Systems Engineering, Daegu Gyeongbuk Institute of Science and Technology (DGIST), Daegu, 711-873, Republic of Korea. *E-mail: sangarajus@dgist.ac.kr., Fax: (+82) 53-785-6409*.

† Electronic Supplementary Information (ESI) available: Experimental details, additional TEM images, additional result. See DOI: 10.1039/b000000x/

1. M. K. Debe, *Nature*, 2012, **486**, 43–51.
2. H. A. Gasteiger and N. M. Marković, *Science*, 2009, **324**, 48–49.
3. G. Cui, L. Zhi, A. Thomas, U. Kolb, I. Lieberwirth, and K. Müllen, *Angew. Chemie - Int. Ed.*, 2007, **46**, 3464–3467.
4. Y. Liu and W. E. Mustain, *J. Am. Chem. Soc.*, 2013, **135**, 530–533.
5. Z. Chen, D. Higgins, A. Yu, L. Zhang, and J. Zhang, *Energy Environ. Sci.*, 2011, **4**, 3167–3192.
6. F. Jaouen, E. Proietti, M. Lefèvre, R. Chenitz, J.-P. Dodelet, G. Wu, H. T. Chung, C. M. Johnston, and P. Zelenay, *Energy Environ. Sci.*, 2011, **4**, 114–130.
7. Z. Zhang, X. Wang, G. Cui, A. Zhang, X. Zhou, H. Xu, and L. Gu, *Nanoscale*, 2014, **6**, 3540–3544.
8. R. Jasinski, *Nature*, 1964, **201**, 1212–1213.
9. Z. Yang, Z. Yao, G. Li, H. Nie, Z. Liu, X. Zhou, X. Chen, and S. Huang, *ACS Nano*, 2012, **6**, 205–211.
10. R. Silva, D. Voiry, M. Chhowalla, and T. Asefa, *J. Am. Chem. Soc.*, 2013, **135**, 7823–7826.
11. D.-W. Wang and D. Su, *Energy Environ. Sci.*, 2014, **7**, 576–591.
12. X. Zhao, J. Zhu, L. Liang, C. Li, C. Liu, J. Liao, and W. Xing, *Appl. Catal. B Environ.*, 2014, **154**, 177–182.
13. H. Liang, X. Zhuang, S. Bru, X. Feng, and K. Mu, *Nat. Commun.*, 2014, **5**, 4973.
14. H. T. Chung, J. H. Won, and P. Zelenay, *Nat. Commun.*, 2013, **4**, 1922.
15. G. Wu, K. L. More, C. M. Johnston, and P. Zelenay, *Science*, 2011, **332**, 443–447.
16. Y. Tan, C. Xu, G. Chen, X. Fang, and N. Zheng, *Adv. Funct. Mater.*, 2012, **22**, 4584–4591.
17. E. Proietti, F. Jaouen, M. Lefèvre, N. Larouche, J. Tian, J. Herranz, and J.-P. Dodelet, *Nat. Commun.*, 2011, **2**, 416.
18. J. Y. Cheon, T. Kim, Y. Choi, H. Y. Jeong, M. G. Kim, Y. J. Sa, J. Kim, Z. Lee, T. Yang, K. Kwon, O. Terasaki, G. Park, R. R. Adzic, and S. H. Joo, *Sci. Rep.*, 2013, **3**, 2715–2723.
19. J. Sanetuntikul, T. Hang, and S. Shanmugam, *Chem. Commun.*, 2014, **50**, 9473–9476.
20. H. Shi, J. N. Reimers, and J. R. Dahn, *J. Appl. Crystallogr.*, 1993, **26**, 827–836.
21. H. Peng, Z. Mo, S. Liao, H. Liang, L. Yang, F. Luo, H. Song, Y. Zhong, and B. Zhang, *Sci. Rep.*, 2013, **3**, 1765.
22. F. Tuinstra, *J. Chem. Phys.*, 1970, **53**, 1126–1130.
23. P. Marcus, *Corros. Sci.*, 1992, **33**, 805–814.
24. B. Jousselme, S. Palacin, A. Morozan, and P. Je, *Phys. Chem. Chem. Phys.*, 2011, **13**, 21600–21607.
25. H. Huang, I. Shown, S. Chang, H. Hsu, H. Du, M. Kuo, K. Wong, S. Wang, C. Wang, L. Chen, and K. Chen, *Adv. Funct. Mater.*, 2012, **22**, 3500–3508.
26. S. Shanmugam and T. Osaka, *Chem. Commun.*, 2011, **47**, 4463–4465.
27. N. K. Chaudhari, M. Y. Song, and J. Yu, *Sci. Rep.*, 2014, **4**, 5221.
28. C. V. Rao, C. R. Cabrera, and Y. Ishikawa, *J. Phys. Chem. Lett.*, 2010, **1**, 2622–2627.
29. A. Kong, X. Zhu, Z. Han, Y. Yu, Y. Zhang, B. Dong, and Y. Shan, *acs Catal.*, 2014, **4**, 1793–1800.
30. L. Feng, L. Yang, Z. Huang, J. Luo, M. Li, D. Wang, and Y. Chen, *Sci. Rep.*, 2013, **3**, 3306.
31. N. Ramaswamy and S. Mukerjee, *Adv. Phys. Chem.*, 2012, **2012**, 1–17.
32. Y. Liang, *Nat. Mater.*, 2011, **10**, 780–786.
33. Y. Chang, F. Hong, C. He, Q. Zhang, and J. Liu, *Adv. Mater.*, 2013, **25**, 4794–4799.
34. I. Kruusenberg, L. Matisen, Q. Shah, A. M. Kannan, and K. Tammeveski, *Int. J. Hydrogen Energy*, 2012, **37**, 4406–4412.

Table of Contents

Fe-N-C exhibited better activity and stability compared with Pt/C in alkaline electrolyte. Fe-N-C showed comparable fuel cell performance with Pt/C.